Structural Features and Light-Dependent Changes in the Sequence 59−75 Connecting Helices I and II in Rhodopsin: A Site-Directed Spin-Labeling Study[†,‡]

Christian Altenbach,[§] Judith Klein-Seetharaman,[||] John Hwa,[||] H. Gobind Khorana,*[,||] and Wayne L. Hubbell*[,§]

Jules Stein Eye Institute and Department of Chemistry and Biochemistry, University of California, Los Angeles, CA 90095-7008, and Departments of Biology and Chemistry, Massachusetts Institute of Technology, 77 Massachusetts Avenue, Cambridge, MA 02139

Received January 4, 1999; Revised Manuscript Received April 8, 1999

ABSTRACT: Twenty-one single-cysteine substitution mutants were prepared in the sequence 56−75 between transmembrane helices I and II at the cytoplasmic surface of bovine rhodopsin. Each mutant was reacted with a sulfhydryl-specific reagent to produce a nitroxide side chain. The electron paramagnetic resonance of the labeled proteins in dodecyl maltoside solution was analyzed to provide the relative mobility and accessibility of the nitroxide side chain to both polar and nonpolar paramagnetic reagents. The results indicate that the hydrophobic−water interface of the micelle intersects helices I and II near residues 64 and 71, respectively. Thus, the sequence 64−71 is in the aqueous phase, while 56−63 and 72−75 lie in the transmembrane helices I and II, respectively. The lipid-facing surfaces on transmembrane helices I and II near the cytoplasmic surface correspond to approximately 180° and 90° of arc on the helical surfaces, respectively. Photoactivation of rhodopsin produced changes in structure in the region investigated, primarily around helix II. However, these changes are much smaller than those noted by spin labels in helix VI (Altenbach, C., Yang, K., Farrens, D., Farahbakhsh, Z., Khorana, H. G., and Hubbell, W. L. (1996) *Biochemistry 35*, 12470).

Rhodopsin, the photoreceptor of the vertebrate retina, is a prototypical member of the large GPCR[1] family (see refs *2*−*4* for reviews). As for all GPCR's the rhodopsin fold is believed to consist of seven transmembrane helices, as shown for the secondary structural model of rhodopsin in Figure 1. Upon activation by light, rhodopsin binds to and activates transducin, the visual G protein. The sequences connecting transmembrane helices III−IV and V−VI, and a sequence connecting transmembrane helix VII with the palmitoylation sites at 322 and 323 (Figure 1) are involved in binding and/or activation of transducin (*12*−*16*). Apparently, photoactivation triggers a conformational change in rhodopsin that presents critical features of these sequences to the G protein. Although there is a great diversity of signals that activate GPCR's, it is likely that the general structural motif and mechanism of activation are conserved throughout the family.

The three-dimensional structure of GPCR's and the nature of the conformational switch leading to activation are areas of much interest. However, due to the general difficulties of crystallization of membrane proteins, no high-resolution structure of any GPCR is available at this time. Rhodopsin remains as the best characterized member of the family. Recently, a model for packing of the rhodopsin helices was proposed (*17*), on the basis of low-resolution electron density

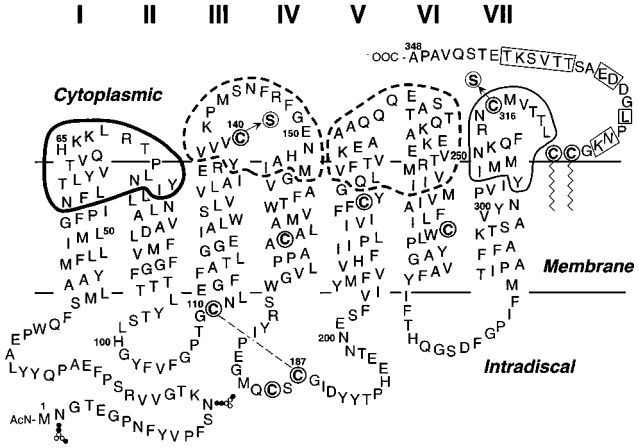

FIGURE 1: A secondary structure model of rhodopsin showing the residues in the cytoplasmic region where single-cysteine substitutions and nitroxide spin labels have been introduced. The sequence investigated by SDSL in the present study is outlined with a bold line. The sequences included within dashed lines were previously investigated (*5*−*8*). The sequences highlighted by a thin line and boxed in the C-terminal domain are the subject of accompanying papers (*1*, *9*−*11*). In all single-cysteine substitution mutants, the reactive native cysteines at residues 140 and 316 were replaced by serine, as indicated. The secondary structure in the sequences connecting the transmembrane helices at the cytoplasmic surface of the membrane, and the points at which the rhodopsin polypeptide crosses the membrane−aqueous interfaces at the cytoplasmic surface, are based on the studies referenced above.

[†] Research reported here was supported by NIH grants EY05216 (W.L.H.) and GM 28289 (H.G.K.), the Jules Stein Professorship Endowment (W.L.H.), and a grant from the Bruce Ford Bundy and Anne Smith Bundy Foundation.

[‡] This is number 33 in the series "Structure and Function of Rhodopsin". The preceding paper is reference *1*.

* To whom correspondence should be addressed

[§] University of California.

[||] Massachusetts Institute of Technology.

[1] Abbreviations: DM, dodecylmaltoside; EPR, electron paramagnetic resonance; GPCR, G-protein-coupled receptor; NiEDDA, Ni(II)-ethylenediaminediacetate; 4-4-PDS, 4,4′-pyridinedisulfide; SDSL, site-directed spin labeling.

10.1021/bi990014l CCC: $18.00
Published on Web 05/26/1999

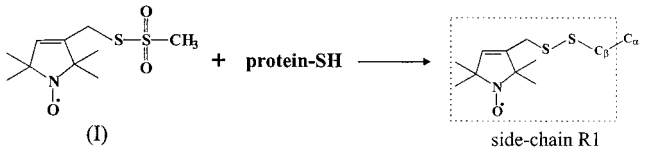

FIGURE 2: Reaction of the methanethiosulfonate spin label (I) to produce the nitroxide side chain designated R1

maps derived from cryo-electron microscopy (*18*). The structures of synthetic peptides corresponding to the extramembranous sequences of rhodopsin at the cytoplasmic surface have been examined in solution by NMR (*19*−*22*), and a model for the structure of the cytoplasmic surface has been proposed (*23*). Pairs of histidines introduced by mutagenesis have been used to explore proximity relationships between the rhodopsin helices by analysis of metal ion effects on function (*24*).

SDSL is an evolving technology that has provided some of the most detailed structural information available on the native rhodopsin molecule, and on light-induced changes in structure. In SDSL, a paramagnetic side chain is substituted in the protein at a selected site. The usual approach is cysteine substitution mutagenesis and modification of the unique sulfhydryl group by a suitable nitroxide reagent. The majority of studies, including the present one, have employed a methanethiosulfonate reagent (I) that generates the nitroxide side chain designated R1 (Figure 2).

The EPR of R1 in a folded protein provides data on the mobility and solvent accessibility of the side chain (see refs *25*−*27* for reviews of the method). "Mobility" is a qualitative descriptor of the dynamic state of R1, measured from features of an EPR spectrum, such as resonance line width and the second moment (*28*). Studies of R1 in T4 lysozyme, a protein of known structure, showed that sites could be categorized according to their topographical location using side chain mobility alone (*28*). For example, helix surface sites, buried sites, loop sites, or tertiary contact sites can be resolved. The solvent accessibility of R1, inferred from the collision frequency of the nitroxide with paramagnetic reagents in solution, provides a similar categorization (*25*−*27*).

If a single R1 residue is moved along a sequence (a "nitroxide scan"), sequence-specific secondary structure can be deduced from the periodicity in mobility and/or accessibility (*26*, *28*, *29*). Local structural information deduced from accessibility and mobility often provides the necessary constraints to discriminate among models for structure.

SDSL has been extensively applied to the investigation of structure and conformational changes at the cytoplasmic surface of rhodopsin. Nitroxide scans through the sequences connecting the III−IV and V−VI transmembrane helices have been carried out (Figure 1). In accompanying papers, nitroxide scans are reported in the C-terminal sequence (*9*) and in helix VII and the extramembranous extension that ends at the palmitorylation sites (*10*). Thus, EPR studies using single-R1 substitutions have now been completed for the entire cytoplasmic face of the molecule. Some of the results from these studies are summarized in Figure 1. For example, the vertical position of each helix relative to the membrane−water interface, the cytoplasmic aqueous extension of each helix, and the orientation of the helices in the rhodopsin fold were deduced from SDSL studies. Of relevance to the rhodopsin conformational switch was the discovery of a helix VI movement upon photoactivation (*8*, *30*), with a smaller movement in helix III (*6*).

In the present study, SDSL is used to explore the structure and dynamics of the sequence connecting transmembrane helices I and II. For this purpose, the single-cysteine mutations in the sequence 56−75 described in a accompanying paper were used (*1*). The results fix the approximate vertical positions of helices I and II with respect to the membrane surface and suggest a specific mapping of the 59−75 sequence onto the electron density contour sections derived from cryoelectron microscopy (*18*). Photoactivated changes in this region of the molecule are small as detected by SDSL, and primarily located in helix II.

EXPERIMENTAL SECTION

Preparation and Spin Labeling of Rhodopsin Mutants. The single-cysteine substitution mutants in the region 56−75 used in this study were prepared and purified in DM solution as described (*1*) and were spin-labeled with (1-oxy-2,2,5,5 tetramethylpyrrolin-3-methyl) methanethiosulfonate (I) (a gift from Prof. Kálmán Hideg, University of Pécs, Hungary) as described elsewhere (*31*). Spin-labeled mutants will be designated by giving the original residue and the sequence number followed by R1, or just the sequence number followed by R1. Thus, H65R1 or 65R1 is a mutant with the native histidine at 313 replaced by the nitroxide side chain R1. The spin-labeled mutants were concentrated in the DM solution and loaded into quartz or TPX capillaries, and X-band EPR spectra and power saturation data were collected as previously described (*32*).

RESULTS

The methanethiosulfonate reagent (I) reacted with each of the single-cysteine substitution mutants in the dark, except 56−58, to produce the distinctive EPR spectra shown in Figure 3 (solid trace). The lack of reaction of (I) with cysteine residues at 56−58 is consistent with their poor reactivity toward another sulfhydryl reagent, 4-PDS (*1*). Photoactivation of rhodopsin produces only small changes in the EPR spectra (Figure 3, dotted trace), suggesting that only minor changes in local structure take place upon formation of the metarhodopsin II intermediate.

For R1 at each site, the mobility and accessibility to collision with O_2 and NiEDDA were determined in the dark state, and the data are shown in Figure 4 (ΔH^{-1} and Π). The mobility is measured here by the inverse width of the central resonance line ($m_I = 0$) of the nitroxide spectrum (*28*). This qualitative measure does not discriminate between populations in cases of multiple components but more heavily weighs the most mobile component. The accessibility of a nitroxide to collision with paramagnetic reagents is measured by the quantity Π, the "accessibility parameter" (*33*, *34*). Π is proportional to the collision frequency of the reagent with the nitroxide. To examine the accessibility of R1 on all surfaces of a membrane protein Π, one needs values for both polar and nonpolar reagents. For the nonpolar reagent, O_2 is selected because it has high solubility in hydrophobic solvents and a reasonable solubility in water. For the polar reagent, NiEDDA is used because it has extremely limited solubility in hydrophobic solvents but very high solubility in water. For R1 at buried sites, both $\Pi(O_2)$ and Π(NiEDDA)

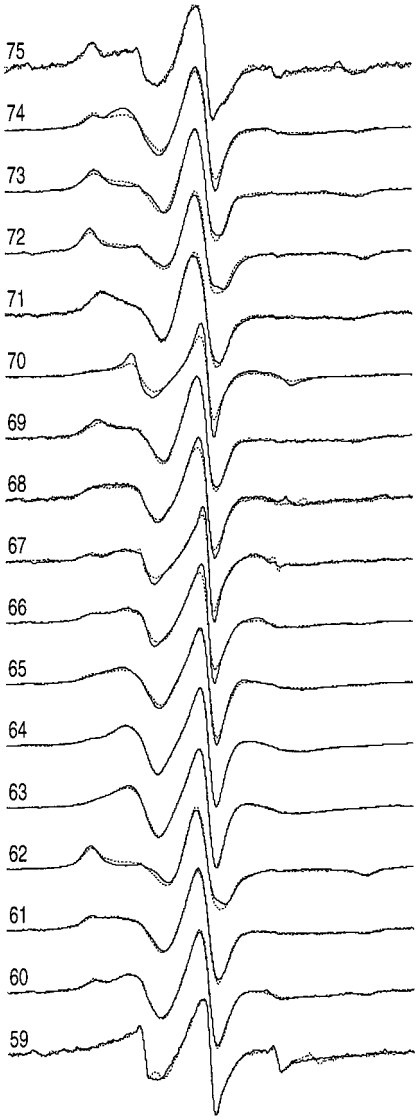

FIGURE 3: EPR spectra in the dark (solid trace) and after photoactivation (dotted trace) for each of the spin-labeled mutants.

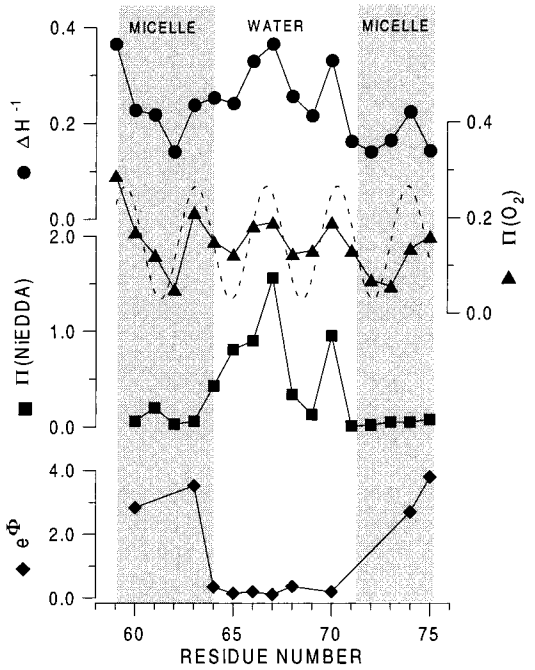

FIGURE 4: Mobility and accessibility of the R1 side chain in the sequence 59−75. The mobility of the R1 side chain measured by the inverse of the central resonance line width, ΔH^{-1} (●). The accessibility to collision with molecular oxygen (▲) and with NiEDDA (■). The concentration of NiEDDA was 20 mM, and for O_2 was that in equilibrium with air. The dotted line has a period of 3.6 residues. The function e^{Φ} for the surface (exposed) and mobile residues (◆).

are low. For exposed sites in the micelle interior, $\Pi(O_2) \gg \Pi$(NiEDDA), and vice versa for exposed sites in the water phase. Figure 4 (▲ and ■, respectively) shows $\Pi(O_2)$ and Π(NiEDDA) for R1 residues in the sequence 59−75.

The function $\Phi = \ln[\Pi(O_2)/\Pi(\text{NiEDDA})]$ is a linear function of depth in the bilayer for an R1 side chain on the surface of a membrane protein and is used as a measure of immersion depth (*34*). However, it can also be used to identify R1 residues on the surface of a membrane protein that lie at the boundary region between a micelle hydrophobic interior and the water phase (*6*, *8*). For R1 residues at the boundary, $\Phi \approx 0$ for O_2 in equilibrium with air and 20 mM Ni(EDDA). For R1 in the aqueous phase, $\Phi < 0$, and for R1 in a micelle or membrane interior, $\Phi > 0$. These criteria apply only to R1 residues exposed at the surface of the protein, where the effect of the size difference between O_2 and NiEDDA is small (*34*).

For purposes of graphical representation, e^{Φ} is preferred for locating the micelle−water boundary, because of the larger changes in this function across the diffuse micelle−water interface. Figure 4 (◆) shows e^{Φ} as a function of sequence position for the residues that have sufficiently high mobility and $\Pi(O_2)$ values to be considered surface-exposed. Between residues 63 and 64, e^{Φ} decreases sharply through 1 ($\Phi \approx 0$) to a value of about 0.125 ($\Phi \approx -2.1$). Thus, residues from 56 to 63 lie in the hydrophobic micelle interior, and residue 64 is the first water-exposed site. R1 residues in the segment 64−70 have an average value of e^{Φ} close to that for completely exposed residues on water-soluble proteins (Altenbach, C., Mchaourab, H. S., Hubbell, W. L., unpublished results) and close to that for R1 in other solvent-exposed sequences in rhodopsin (*6*, *8*). Thus, 64−70 is the aqueous-solvated portion of the sequence. Between residues 70 and 74, the segment again crosses the micelle boundary, probably near residue 71. The exact crossing position is uncertain, because many of the R1 residues in this region are immobilized and unsuitable for analysis of Φ. We tentatively conclude that the segment 71−75 crosses the boundary from water to the hydrophobic micelle interior.

The values of $\Pi(O_2)$ are clearly periodic as a function of position throughout the sequence, with a period of 3.6, that of a α-helix (Figure 4 (▲)). At most residues, the mobility, measured by ΔH^{-1}, mirrors $\Pi(O_2)$ reasonably well, with the same period and phase. Thus, the most inaccessible residues are generally also the most immobilized. However, the entire segment from 59 to 75 cannot be a continuous helix. The interpretation of these results in terms of secondary structure will be discussed below.

The very low values of Π(NiEDDA) at all residues in the micelle interior are due to the low solubility of NiEDDA in that region. For R1 residues in the water-exposed segment from 64 to 70, Π(NiEDDA) reflects $\Pi(O_2)$ reasonably well, and both measures reveal the high accessibility of the residues, except for 68R1 and 69R1. The low accessibility

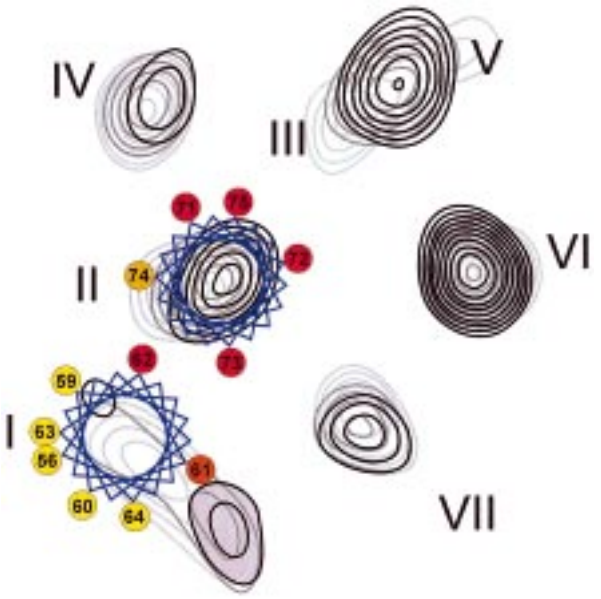

FIGURE 5: Residue positions of the proposed helical segments from 59 to 64 and from 71 to 75 mapped onto electron density contour sections taken at 13, 15, and 17 Å from the center of the membrane. The dots mark the locations of the α-carbon atom of the residue. The dots are coded on a red to yellow scale according to mobility and accessibility, red being the most immobilized and inaccessible. The numbering of the rhodopsin helices in the electron density map is from refs *17* and *18* and corresponds to the 13 Å section (lightest traces) where the helices are well-resolved. In the 17 Å section (darkest traces), the densities for helices III and V have merged. The contour sections were from a three-dimensional map at an effective resolution of 7.5 Å in the membrane plane and 16.5 Å normal to the plane and were kindly provided by G. F. X. Schertler (personal communication).

at these latter sites is consistent with their low mobility (Figure 4 (●)) and indicates that the sequence makes tertiary contact with other ordered regions in the cytoplasmic surface of rhodopsin.

DISCUSSION

The data presented above define the residues at which the micelle−water interface intersects the sequences corresponding to the putative helices I and II in rhodopsin. These residues are shown in the secondary structure model of Figure 1, where it is assumed that the boundary is the same in the micelle and bilayer states, although this remains to be verified.

What is the structure of the segment 59−75, extending between the boundaries of transmembrane helices I and II at the cytoplasmic surface of the rhodopsin molecule? Consider first the hydrophobic sequences in the core of the micelle (or membrane). The periodicity of both $\Pi(O_2)$ and mobility are consistent with α-helical structures (Figure 4), although the segments are too short to prove the point by periodicity arguments alone. The possibility of helical structures for the hydrophobic segments 59−64 and 71−75 is further explored in Figure 5. This figure shows the SDSL data mapped onto superposed electron density contour sections from 13, 15, and 17 Å from the center of the membrane. This is approximately the range corresponding to the sequence 59−75 in the native protein (*17*). An excellent correspondence between side chain mobility and accessibility and the electron density maps is obtained assuming helical segments from 59 to 64 and 71 to 75. Thus in helix I, all of the mobile and accessible residues (yellow circles) fall on the outer surface of the putative helix. The single buried residue (red circle) at 62 is in direct contact with helix II. Residue 61R1 is intermediate in both mobility and accessibility. It is interesting to note that this site faces a diffuse electron density of uncertain origin that could be due to the C-terminal extension (violet-shaded region) (*18*). The partial immobilization is consistent with matter in that general area.

In helix II, all substituted residues but 74R1 are immobile and inaccessible, suggesting that most of the surface of the transmembrane segment is buried in the protein core near the cytoplasmic interface. This is in striking contrast with helix I, where the hydrophobic face corresponds to at least 180° of the arc on the helix surface. This clear distinction between helices I and II matches the electron density contours, supporting the residue mapping shown in Figure 5.

Baldwin et al. (*17*) proposed a α-carbon structural model for the rhodopsin helices on the basis of a sequence analysis of GPCR's and the electron density map of Unger et al. (*18*). In this model, helix I crosses the membrane−aqueous interface at residue Y60, approximately 14 Å from the center of the membrane, and extends to residue Q64. The SDSL data suggests that the crossing point is at Q64 in the DM micelle. In Figure 5, helix I is also terminated at Q64. If the helix were to continue, residue 65 would be located at the buried surface, facing the interface between helices II and VII. However, 65R1 is a relatively mobile residue, and 65C has high reactivity with 4-PDS (*1*). Therefore, 65 is not likely to be located at a packed interface between helices. The Baldwin model begins helix II at residue 69 and places the lipid boundary at residue 73. The SDSL data alone cannot locate the beginning of helix II, because the accessibility and mobility maintain a periodic dependence on sequence position throughout the sequence. However, the accessibility data shows that the sequence enters the hydrophobic interior of the micelle in the region 70−74, and on thermodynamic grounds, the helix probably begins at or before this range. Because proline has a high propensity to be in the first turn at the N terminus of a helix (*35*), the helix is suggested to begin at P71, as shown in Figure 5. However, the SDSL data would agree equally well with residue 69 as the origin of helix II.

Both SDSL and an analysis of residue variability among GPCR sequences (*17*) agree that residue 62 is located on the buried surface of helix I, while 59, 60, 63, and 64 are on the solvent-exposed surface of the helix. Residue 61 may be at an interface between these extremes. For helix II, both the model and SDSL place 71, 72, 73, and 75 at the buried surface of the helix and 74 at the solvent-exposed surface.

In an accompanying paper, the rates of reaction of cysteine residues substituted at positions 60−74 with 4-PDS are reported (*1*). In helix I, residues 61C and 62C have a low reactivity, while 60, 63, and 64 have high reactivity, consistent with their assignments in Figure 5. In helix II, the comparison is more interesting. Here, 74C is of modest reactivity, again consistent with the SDSL data which place 74 on the outer surface of the helix. However, SDSL and sequence analysis (*17*) place residues 72 and 73 at the buried surface of helix, although they have relatively high reactivity.

A similar situation was found for residues 310 and 313 on helix VII. These residues appear to be buried in the structure according to SDSL but react rapidly with 4-PDS (*10*, *11*). It is significant that 72, 73, 310, and 313 all face the same cavity in the rhodopsin molecule.

Thus, sulfhydryl reactivity suggests that sites 72, 73, 310, and 313 are solvent-exposed, while SDSL data indicates that they are buried within the protein. In an accompanying paper, a model was offered to account for this striking difference (*11*). The major point was that reactivity can be relatively high at a buried site if structural fluctuations provide a conformational substate with the SH group exposed. SDSL analysis may not resolve this state if it is a minor population. Thus, in the context of this model, the results suggest the existence of structural fluctuations that lead to accessibility in the cavity between helices II and VII.

Recently, the solution structure of a synthetic peptide corresponding to residues 60−76 of rhodopsin was determined by 2D NMR methods (*21*). The reported structure is U-shaped with an unusually stable β-turn in the center and "frayed" ends. The absence of helical structures at the ends suggested to the authors that no part of the sequence is contained within either helix I or II in the native protein. This would mean that Y60 is beyond helix I and that L76 lies before the beginning of helix II. These conclusions are somewhat different than those reached here. As discussed above, both SDSL and sequence analysis indicate that helix I extends to about residue Q64, one turn beyond Y60, and helix II begins around 69−71, nearly two turns before L76. The SDSL data further suggest that Q64 is the first residue of the sequence to be in the aqueous phase, and P71 would already be in the membrane interior. The NMR structure identifies 64−69 as a stable β-turn in the aqueous phase, and the SDSL data could be consistent with this assignment.

Photoactivation of rhodopsin leads to minor changes in mobility of R1 at sites in helix I and in the water-exposed portion of the sequence. Larger changes are seen in helix II in the region 70R1−74R1 (Figure 3), although these are still small compared to those in helix VI (*8*, *30*). The kinetics of thiopyridone release from 4-PDS-labeled rhodopsin cysteine mutants by DTT revealed a similar pattern of light effects; that is, larger effects were observed in helix II (*1)*. However, the effects of photoactivation on the kinetics of thiopyridone release were much larger than on the mobility of R1 residues at the same sites, judging by the small changes in the EPR spectra. This difference might again be accounted for by the fundamental difference in the features that determine reactivity and mobility, as discussed in an accompanying paper (*11*) and above.

REFERENCES

1. Klein-Seetharaman, J., Hwa, J., Cai, K., Altenbach, C., Hubbell, W. L. and Khorana, H. G. (1999) *Biochemistry 38*, 7938−7944.
2. Helmreich, E. J. M., and Hofmann, K.-P. (1996) *Biochim. Biophys. Acta 1286*, 285−322.
3. Wess, J. (1997) *FASEB J. 11*, 346−354.
4. Sakmar, T. P. (1998) *Prog. Nucleic Acid Res. Mol. Biol. 59*, 1−34.
5. Ridge, K. D., Zhang, C., and Khorana, H. G. (1995) *Biochemistry 34*, 8804−8811.
6. Farahbakhsh, Z., Ridge, K. D., Khorana, H. G., and Hubbell, W. L. (1995) *Biochemistry 34*, 8812−8819.
7. Yang, K., Farrens, D. L., Hubbell, W. L., and Khorana, H. G. (1996) *Biochemistry 35*, 12464−12469.
8. Altenbach, C., Yang, K., Farrens, D. F., Farahbakhsh, Z., Khorana, H. G., and Hubbell, W. L. (1996) *Biochemistry 35*, 12470−12478.
9. Langen, R., Cai, K., Altenbach, C., Khorana, H. G., and Hubbell, W. L. (1999) *Biochemistry 38*, 7918−7924.
10. Cai, K., Klein-Seetharaman, J., Farrens, D., Zhang, C., Altenbach, C., Khorana, H. G., and Hubbell, W. L. (1999) *Biochemistry 38*, 7925−7930.
11. Altenbach, C., Cai, K., Khorana, H. G., and Hubbell, W. L. (1999) *Biochemistry 38*, 7931−7937.
12. Kuhn, H., and Hargrave, P. A. (1981) *Biochemistry 20*, 2410−2417.
13. Konig, B., Arendt, A., McDowell, J. H., Kahlert, M., Hargrave, P. A., and Hofmann, K. P. (1989) *Proc. Natl. Acad. Sci. U.S.A. 86*, 6878−6882.
14. Franke R. R., Konig, B., Sakmar, T. P., Khorana, H. G., and Hofmann, K. P. (1990) *Science 250*, 123−125.
15. Franke, R. R., Sakmar, T. P., Graham, R., and Khorana, H. G. (1992*) J. Biol. Chem. 267*, 14767−14774.
16. Ernst, O. P., Hofmann, K. P., and Sakmar, T. P. (1995) *J. Biol. Chem. 270*, 10580−10586.
17. Baldwin, J., Schertler, G. F. X., and Unger, V. M. (1997) *J. Mol. Biol. 272*, 144−164.
18. Unger, V. M., Hargrave, P. A., Baldwin, J. M., and Schertler, G. F. X. (1997) *Nature 389*, 203−206.
19. Yeagle, P. L., Alderfer, J. L., and Albert, A. D. (1995) *Biochemistry 34*, 14621−14625.
20. Yeagle, P. L., Alderfer, J. L., and Albert, A. D. (1995) *Nat. Struct. Biol. 2*, 832−834.
21. Yeagle, P. L., Alderfer, J. L., and Albert, A. D. (1996) *Mol. Vis. 2*, 12.
22. Yeagle, P. L., Alderfer, J. L., and Albert, A. D. (1997) *Biochemistry 36*, 3864−3869.
23. Yeagle, P. L., Alderfer, J. L., and Albert, A. D. (1997) *Biochemistry 36*, 9649−9654.
24. Sheikh, S. P., Zvyaga, T. A., Lichtarge, O., Sakmar, T. P., and Bourne. H. R. (1996) *Nature 383*, 347−350.
25. Hubbell, W. L., and Altenbach, C. (1994) *Curr. Opin. Struct. Biol. 4*, 566−573.
26. Hubbell, W. L., Mchaourab, H. S., Altenbach, C., and Lietzow, M. (1996) *Structure 4*, 779−782.
27. Hubbell, W. L., Gross, A., Langen, R., and Lietzow, M. (1998) *Curr. Opin. Struct. Biol. 8*, 649−656.
28. Mchaourab, H. S., Lietzow, M. A., Hideg, K., and Hubbell, W. L. (1996) *Biochemistry 35*, 7692−7704.
29. Altenbach, C., Marti, T., Khorana, H. G., and Hubbell, W. L. (1990) *Science 248*, 1088−1092.
30. Farrens, D. L., Altenbach, C., Yang, K., Hubbell, W. L., and Khorana, H. G. (1996) *Science 274*, 768−770.
31. Resek, J. F., Farahbakhsh, Z., Hubbell, W. L., and Khorana, H. G. (1993) *Biochemistry 32*, 12025−12031.
32. Altenbach, C., Flitsch, S., Khorana, H. G., and Hubbell, W. L. (1989) *Biochemistry 28*, 7806−7812.
33. Farahbakhsh, Z., Altenbach, C., and Hubbell, W. L. (1992*) Photochem. Photobiol. 56*, 1019−1033.
34. Altenbach, C., Greenhalgh, D., Khorana, H. G., and Hubbell, W. L. (1994) *Proc. Natl. Acad. Sci. U.S.A. 91*, 1667−1671.
35. Richardson, J. S., and Richardson, D. C. (1989) in *Prediction of Protein Structure and the Principles of Protein Conformation* (Fasman, G. D., Ed.) p 1, Plenum Press, New York and London.

BI990014L